Modelling of sediment transport and bed deformation in rivers with continuous bends*

Hefang Jing[a†] *Chunguang Li*[a] *Yakun Guo*[b] *Lixiang Zhang*[c] *Lijun Zhu*[d] *Yitian Li*[e]

[a] Res. Inst. Numer. Comput. & Eng. Appl., Beifang University of Nationalities, Yinchuan 750021, China.
[b] School of Engineering, University of Aberdeen, Aberdeen, AB24 3UE, UK.
[c] Department of Engineering Mechanics, Kunming University of Science and Technology, Kunming, 650051, China.
[d] School of Information and Computing Science, Beifang University of Nationalities, Yinchuan 750021, China.
[e] State Key Laboratory of Water Resources and Hydropower Engineering Sciences, Wuhan University, Wuhan 430072, China.

Abstract

A two dimensional (2D) RNG k-ε sediment model including the effects of secondary currents is developed to simulate sediment transport and bed deformation in rivers with continuous bends. Nonuniform suspended and bedload sediment transports and variation of effective bed material size distribution are included in the model. A semi-coupled scheme for sediment model is proposed, which can be used for simulating both the long- and short-term sediment transport whenever riverbed changes. The model is applied to simulate the flow and sediment transport in the Shapotou reservoir in the upper reach of the Yellow River which is a typical natural river reach with continuous bends. River bed deformations caused by suspended and bedload sediment transport are investigated. Good agreement between the numerically simulated results and the field measurements is obtained, indicating that the model is capable of simulating the sediment transport and predicting the bed deformation of rivers having continuous bends with reasonable accuracy.

Key words: RNG k-ε turbulence model, bed deformation，suspended sediment, bedload sediment,

* **Grant sponsor:** the Major Research Plan Project, National Natural Science Foundation of China (grant number: 91230111 and 51279071); National Key Basic Research Development Program of China (973 Program, grant number: 2010CB429002); Project of Science and Technology of Colleges in Ningxia, China (grant number: NGY2012097); Project of Beifang University of Nationalities, China (grant number: 2012XZK05); Foreign Expert Project of Beifang University of Nationalites, China.

† Address for Correspondence: Dr. Hefang Jing, Res. Inst. Numer. Comput. & Eng. Appl., Beifang University of Nationalities, Yinchuan 750021, China. Email: jinghef@163.com. Tel: +86 951 2068011

bed material granularity

NOMENCLATURE			
C	Chezy coefficient	h	water depth
D_{50}	medium diameter of bed material	k	turbulent kinetic energy
P_{mL}	bed material granularity	n	Manning coefficient
$P_{mL,0}$	original bed material granularity	u	velocity in x direction
S	sediment concentration	v	velocity in y direction
S_L	group sediment concentration	z	water level
S_v	sediment concentration by volume	α_L	group saturation recovery coefficient of sediment
S^*	sediment carrying capacity	γ	water specific gravity
S_L^*	group sediment carrying capacity	γ'	dry specific gravity of sediment
$\overline{U}$	depth averaged velocity	κ	Karman constant
Z	bed elevation	ε	turbulence dissipation rate
$Z_{S,L}$	the deposition thickness of the L-th group suspended sediment	ν	water viscosity
$Z_{b,L}$	the deposition thickness of the L-th group bedload	ν_t	water eddy viscosity
d_{50}	medium diameter of suspended sediment	γ_s	sediment specific gravity
d_m	averaged diameter of suspended sediment	γ_m	Specific gravity of muddy water
d	diameter of sediment	ω	sediment settling velocity
g	gravity acceleration	ω_L	sediment settling velocity of the L-th group sediment

1. Introduction

Flow and sediment transport near hydraulic structures in rivers have been extensively studied using various approaches, such as theoretical analysis, laboratory experiments, field measurements and numerical simulation. Among these approaches, numerical simulation has advantages in several aspects and has been increasingly used (Falconer 1992; Guo *et al.* 2007). In natural rivers,

horizontal scale is usually much greater than vertical scale; therefore, it is suitable to apply depth averaged two dimensional (2D) models (Guo *et al.* 2012). Generally speaking, numerical simulation using these models not only requires less computational time than three dimensional (3D) sediment models (particularly for large scale simulation), but also is more accurate than that of 1D sediment models. As a result, depth averaged 2D sediment models are widely applied in engineering to study sediment transport and river bed deformation. Nagata *et al.* (2000) developed a 2D sediment model for inviscid river banks. Hung *et al.* (2009) developed an unsteady 2D depth-averaged model for nonuniform sediment transport in alluvial channels, taking the transport mechanisms of cohesive and noncohesive sediment, suspended sediment and bedload into account. Duan and Julien (2010) conducted 2D numerical simulation for a laboratory bend, considering transport of suspended sediment and bedload, and river bed deformation. Li and Millar (2011) developed a 2D morphodynamic model of gravel-bed river with floodplain vegetation, considering the effects of riparian and floodplain vegetation on bank strength, floodplain flow resistance, shear stress partitioning, and bedload transport. Serrano-Pacheco *et al.* (2012) conducted 2D bedload transport simulations, in which bedload transport is governed by a power law of flow velocity and by a flow/sediment interaction parameter.

Though these 2D sediment models have been widely used to simulate the sediment transport and bed deformation in rivers and open channels, many of them are either laminar model, or zero equation turbulent model or standard k-ε turbulent model. As such, they cannot be applied to simulate the complicated turbulent flow and sediment transport in rivers with continuous bends in which the effect of secondary currents induced by the bends or curved channels is important.

Some models were modified and taken the effect of secondary currents into account, but they can only be applied to simulate the regular bends in laboratory open channels, and are difficult to be applied to simulate the flow and sediment transport in natural rivers with continuous bends under investigation. Therefore, these 2D sediment models need to be improved before they can be applied to simulate the natural rivers with continuous curves.

The RNG k-ε model, developed from standard k-ε model (Versteeg and Malalasekera,1995), has the advantages over the standard k-ε model. For example, it is more accurate by adding an extra term in the ε-equation; can be used to simulate the turbulent eddy with high accuracy and is applicable to simulate the flows of both the high and low Reynolds number (Jing et al. 2009, 2011). In this study, a 2D depth averaged RNG k-ε sediment model is developed to simulate the flow and sediment transport in the Shapotou reservoir at the upper reach of the Yellow River with continuous bends. The effect of secondary current on flow transport is taken into account in the turbulent model. Both the non-uniform suspended and non-uniform bedload sediment transport is included in the model. In addition, the variation of size distribution of effective bed materials is also simulated in the model. Depth averaged velocity, water level, transport of suspended sediment and bed deformation caused by suspended and bedload sediment transports are investigated.

The governing equations of sediment models can be divided into two modules: flow module and sediment module. The first module includes flow continuous equation, momentum equations and turbulence equations, while the second module includes transportation equations of suspended

sediment and bedload and bed deformation equations. Therefore, there are two basic schemes to numerically solve sediment models, i.e. coupled scheme and decoupled scheme. In the coupled scheme, the flow and sediment modules are solved simultaneously, while in the decoupled scheme, the flow module is solved first, then the sediment module. In other words, in the decoupled scheme, the flow module will no longer be run after the sediment module starts. Generally speaking, the coupled scheme is suitable for short time numerical simulation with the rapid change of the river bed. It is usually not suitable for long time numerical simulation of sediment transport due to the large CPU time consuming. On the other hand, the decoupled scheme is suitable for long time numerical simulation with the slow variation of river bed as it requires less computing time. Usually, the hydraulic elements, such as water level and velocity, change very slightly in the long time numerical simulation of sediment transport when river bed changes slowly. In this situation, it is not necessary to calculate the flow module every time step from the point of view of computing cost. However, after a certain time steps of running the sediment module, the river bed deformation accumulates to a degree that can significantly affect the flow elements. In this situation, the flow module needs to be run to account the effect of sediment transport and bed deformation on the flow field. However, in the decoupled scheme, the flow module is stopped forever after sediment module begins to run. Therefore, the decoupled scheme is unreasonable and needs to be improved in order to simulate the effect of the sediment transport on the flow field. This is one of the motivations of this work in which a semi-coupled scheme is developed by combining the advantages of coupled and decoupled schemes. In the proposed scheme, the sediment module keeps running, while the flow module runs intermittently. Therefore, the scheme is efficient and is less time consuming than the coupled scheme and is more accurate than the

decoupled scheme. The semi-coupled scheme is not only suitable for simulating both the long and short time sediment transport, but is also capable of treating both the rapid and slow change of the river bed.

2. Mathematical model

2.1. The 2D depth averaged RNG k-ε model in Cartesian coordinate

The 2D depth averaged RNG *k-ε* sediment model includes two basic modules: hydraulic module and sediment module. The hydraulic module consists of the following equations (Versteeg and Malalasekera, 1995; Duan and Nanda 2006; Serrano-Pacheco, *et al.* 2012):

$$\frac{\partial z}{\partial t}+\frac{\partial (hu)}{\partial x}+\frac{\partial (hv)}{\partial y}=0 \tag{1}$$

$$\frac{\partial (hu)}{\partial t}+\frac{\partial (huu)}{\partial x}+\frac{\partial (huv)}{\partial y}=\frac{\partial }{\partial x}\left(\nu_e h\frac{\partial u}{\partial x} \right)+\frac{\partial }{\partial y}\left(\nu_e h\frac{\partial u}{\partial y} \right)-gh\frac{\partial z}{\partial x}-\frac{gn^2u\sqrt{u^2+v^2}}{h^{1/3}} \tag{2}$$

$$\frac{\partial (hv)}{\partial t}+\frac{\partial (hvu)}{\partial x}+\frac{\partial (hvv)}{\partial y}=\frac{\partial }{\partial x}\left(\nu_e h\frac{\partial v}{\partial x} \right)+\frac{\partial }{\partial y}\left(\nu_e h\frac{\partial v}{y} \right)-gh\frac{\partial z}{\partial y}-\frac{gn^2v\sqrt{u^2+v^2}}{h^{1/3}} \tag{3}$$

$$\frac{\partial (hk)}{\partial t}+\frac{\partial (huk)}{\partial x}+\frac{\partial (hvk)}{\partial y}=\frac{\partial }{\partial x}\left(\alpha_k \nu_e h\frac{\partial k}{\partial x} \right)+\frac{\partial }{\partial y}\left(\alpha_k \nu_e h\frac{\partial k}{\partial y} \right)+h(P_k+P_{kv}-\varepsilon) \tag{4}$$

$$\frac{\partial (h\varepsilon)}{\partial t}+\frac{\partial (hu\varepsilon)}{\partial x}+\frac{\partial (hv\varepsilon)}{\partial y}=\frac{\partial }{\partial x}\left(\alpha_\varepsilon \nu_e h\frac{\partial \varepsilon}{\partial x} \right)+\frac{\partial }{\partial y}\left(\alpha_\varepsilon \nu_e h\frac{\partial \varepsilon}{\partial y} \right)+h\left[\frac{\varepsilon}{k}(C_{1\varepsilon}^{*}P_k-C_{2\varepsilon}\varepsilon)+P_{\varepsilon v} \right] \tag{5}$$

And the sediment module includes the following equations:

$$\frac{\partial hS_L}{\partial t}+\frac{\partial huS_L}{\partial x}+\frac{\partial hvS_L}{\partial y}=\frac{\partial }{\partial x}\left(\nu_e h\frac{\partial S_L}{\partial x} \right)+\frac{\partial }{\partial y}\left(\nu_e h\frac{\partial S_L}{\partial y} \right)-\alpha_L\omega_L(S_L-S_L^{*}) \tag{6}$$

$$\gamma_s{}'\frac{\partial Z_{S,L}}{\partial t}=\alpha_L\omega_L(S_L-S_L^{*}) \tag{7}$$

$$\gamma'_s \frac{\partial Z_{b,L}}{\partial t} + \frac{\partial g_{bx,L}}{\partial x} + \frac{\partial g_{by,L}}{\partial y} = 0 \tag{8}$$

$$\gamma'_s \frac{\partial E_m P_{mL}}{\partial t} + \alpha_L \omega_L (S_L - S_L^*) + \frac{\partial g_{bx,L}}{\partial x} + \frac{\partial g_{by,L}}{\partial y} + \gamma'_s [\varepsilon_1 P_{mL} + (1-\varepsilon_1) P_{mL,0}] \left(\frac{\partial z_b}{\partial t} - \frac{\partial E_m}{\partial t} \right) = 0 \tag{9}$$

In above equations: z=the water level; *h*=the water depth; *u*, *v*= the vertically averaged velocities in x, y directions, respectively; *t*=the time; *k*= the turbulent kinetic energy; ε =the turbulence dissipation rate; *g*=the acceleration of gravity; *n*=the Manning's coefficient; S_L, $S_L^*, \omega_L, \alpha_L$ =the *L*-th group sediment concentration, sediment carrying capacity, settling velocity, saturation recovery coefficient, respectively; $Z_{S,L}$ =the deposition thickness of the *L*-th group suspended sediment, γ_s' =the dry specific gravity of sediment; $Z_{b,L}, g_{bx,L}$ and $g_{by,L}$ =deposition thickness, discharge per unit width in x and y directions of the *L*-th group bed load, respectively; P_{mL} and $P_{mL,0}$ =bed material granularity and original bed material granularity, respectively; z_b =the bed level, E_m =the thickness of active layer; $\varepsilon_1 = 0$ (if the original river bed is scoured) or $\varepsilon_1 = 1$ (if the original river bed is deposited).

In (1)-(6), the effective viscosity (ν_e) is the sum of the viscosity of water (ν) and the eddy viscosity coefficient of water (ν_t). The values and the calculation of some coefficients such as $\nu_t, P_k, P_{kv}, P_{\varepsilon v}, C_{1\varepsilon}^*, C_\mu, \alpha_k, \alpha_\varepsilon$, can be found in (Yakhot and Orzag, 1986; Rodi 1993).

2.2. Modified 2D depth averaged RNG k-ε model in body fitted coordinates

As the river reach under investigation consists of several irregular bends where strong circulation flow exists, the 2D depth averaged RNG *k*-ε sediment model usually can not reflect the influence of such flow. Therefore, the model needs to be modified to take the influence of circulation flow

into account.

To facilitate the description, the general control equations of the 2D depth averaged RNG *k-ε* sediment model is written in the body fitted coordinate system (BFC):

$$\frac{\partial}{\partial t}(h\Phi)+\frac{1}{J}\frac{\partial}{\partial \xi}(hU\Phi)+\frac{1}{J}\frac{\partial}{\partial \eta}(hV\Phi)=\frac{1}{J}\frac{\partial}{\partial \xi}(\frac{\alpha h\Gamma_{\Phi}}{J}\frac{\partial \Phi}{\partial \xi})+\frac{1}{J}\frac{\partial}{\partial \eta}(\frac{\gamma h\Gamma_{\Phi}}{J}\frac{\partial \Phi}{\partial \eta})+S_{\Phi}(\xi,\eta) \quad (10)$$

where general variable Φ represents 1, u, v, k, ε, S_L in (1)-(6), respectively; ξ and η = the curvilinear coordinates along river bank direction and perpendicular to the river bank direction, respectively; J,α,β,γ = transformation factors, $J=x_{\xi}y_{\eta}-x_{\eta}y_{\xi}$, $\alpha=x_{\eta}^2+y_{\eta}^2$, $\beta=x_{\xi}x_{\eta}+y_{\xi}y_{\eta}$, $\gamma=x_{\xi}^2+y_{\xi}^2$; U and V = components of inverter velocity in ξ and η directions, respectively, $U=uy_{\eta}-vx_{\eta}$, $V=-uy_{\xi}+vx_{\xi}$; Γ_{Φ} = general diffusion coefficient; the source terms of the momentum equations (Eq.s (2) and (3)) are as following:

$$S_u=-\frac{1}{J}gh(z_{\xi}y_{\eta}-z_{\eta}y_{\xi})-\frac{1}{J}\frac{\partial}{\partial \xi}\left(\frac{\beta\Gamma_u h}{J}\frac{\partial u}{\partial \eta}\right)-\frac{1}{J}\frac{\partial}{\partial \eta}\left(\frac{\beta\Gamma_u h}{J}\frac{\partial u}{\partial \xi}\right)-\frac{gn^2u\sqrt{u^2+v^2}}{h^{1/3}} \quad (11)$$

$$S_v=-\frac{1}{J}gh(-z_{\xi}x_{\eta}+z_{\eta}x_{\xi})-\frac{1}{J}\frac{\partial}{\partial \xi}\left(\frac{\beta\Gamma_v h}{J}\frac{\partial v}{\partial \eta}\right)-\frac{1}{J}\frac{\partial}{\partial \eta}\left(\frac{\beta\Gamma_v h}{J}\frac{\partial v}{\partial \xi}\right)-\frac{gn^2v\sqrt{u^2+v^2}}{H^{\frac{1}{3}}} \quad (12)$$

To simulate the influence of circulation flow of bend, extra source terms need to be added in the momentum equations. These new source terms are as following (Lien, et al, 1999):

$$S_u^{new}=S_u+M_u\,,\quad S_v^{new}=S_v+M_v \quad (13)$$

in which the extra source terms can be calculated by

$$M_u=-\frac{1}{J^2}\frac{u\sqrt{\gamma}}{\sqrt{u^2+v^2}}\frac{\partial}{\partial \eta}\left(|\bar{u}|\bar{u}\phi\right),\quad M_v=-\frac{1}{J^2}\frac{v\sqrt{\gamma}}{\sqrt{u^2+v^2}}\frac{\partial}{\partial \eta}\left(|\bar{u}|\bar{u}\phi\right) \quad (14)$$

where $\phi=\sqrt{\frac{\gamma}{\alpha}}\frac{h^2}{R_{\eta}}k_{TS}$, $\bar{u}=\frac{ux_{\xi}+vy_{\xi}}{\sqrt{\gamma}}$, $\bar{v}=\frac{ux_{\eta}+vy_{\eta}}{\sqrt{\alpha}}$, R_{η} = the curvature radius of river bend, k_{TS}= the lateral exchange coefficient due to circulation flow and can be calculated by

158 $$k_{TS} = 5\frac{\sqrt{g}}{\kappa C} - 15.6\left(\frac{\sqrt{g}}{\kappa C}\right)^2 + 37.5\left(\frac{\sqrt{g}}{\kappa C}\right)^3 \quad (15)$$

159 where κ = Karman constant which is related to the sediment concentration (see below), C =

160 Chezy coefficient.

161 $$\kappa = 0.4[1 - 4.2(0.365\text{-}S_v)\sqrt{S_v}] \quad (16)$$

162 where S_v =the sediment concentration by volume.

163

164 The following key parameters need to be determined before the model can be applied for

165 simulation. .

166

167 ***2.3. Suspended sediment carrying capacity***

168 Considering the effect of sediment concentration on Karman constant and silt deposition, Zhang

169 and Zhang（1992）presented a semi-empirical and semi-theoretical formula to calculate suspended

170 sediment carrying capacity based on the relationship between energy consumption of flow and the

171 power require to float sediment. Being verified by broad range of measured data in the Yellow

172 River, the formula has a high adaptability and can be used in the Upper Yellow River. The total

173 suspended sediment carrying capacity can be calculated as following:

174 $$S^* = 2.5\left[\frac{(0.0022 + S_v)\overline{U}^3}{\kappa\frac{\gamma_s - \gamma_m}{\gamma_m} gh\omega_s}\ln\left(\frac{h}{6D_{50}}\right)\right]^{0.62} \quad (17)$$

175 where $\overline{U}$ =vertical mean velocity; D_{50}= medium diameter of bed material; γ_s, γ_m =specific

176 gravity of sediment and muddy water, respectively; ω_s =group setting velocity. The units system

177 adopted is *kg*, *m* and *s*.

The group sediment carrying capacity S_L^* is obtained by multiplying S^* with p_L^* (the graduation of group sediment carrying capacity):

$$S_L^* = p_L^* S^* \tag{18}$$

and p_L^* can be calculated by (Zhang, 1988):

$$p_L^* = wp_L + (1-w)p_{bL}^{'} \tag{19}$$

where P_L=graduation of suspended sediment at inlet; $p_{bL}^{'}$ =related to the graduation of bed material; w=weight factor, and its value ranges from 0.62 to 0.85 when the river bed is silted; from 0.64 to 0.86 when the river bed is scoured; and from 0.49 to 0.52 when the river bed keeps the balance of erosion and deposition.

2.4. Sediment setting velocity

The sediment setting velocity is a very important parameter in the sediment model. There are a lot of formulae to calculate sediment setting velocity, among which the formula developed by Zhang (1988) is one of the most representative formulae that are suitable for the sediment in the Yellow River. According to Zhang (1988), the single grain sediment setting velocity in clean water can be calculated as:

$$\omega_0 = \begin{cases} \dfrac{1}{25.6}\dfrac{\gamma_s-\gamma}{\gamma} g \dfrac{d^2}{\nu}, & \text{for } d \le 0.1mm \\ 1.044\sqrt{\dfrac{\gamma_s-\gamma}{\gamma} gd}, & \text{for } d \ge 4mm \\ \sqrt{\left(13.95\dfrac{\nu}{d}\right)^2 + 1.09\dfrac{\gamma_s-\gamma}{\gamma} gd} - C_1\dfrac{\nu}{d}, & \text{for } 0.1mm < d < 4mm \end{cases} \tag{20}$$

where ω_0 = the sediment setting velocity in clear water, d = the diameter of single grain sediment.

The sediment concentration in the Yellow River is usually high, which will affect the sediment setting velocity. Therefore, the formula must be modified to take the effect of sediment concentration into account. According to Zhang and Zhang (1992), the sediment setting velocity in muddy water can be estimated as:

$$\omega = \omega_0 \left[\left(1 - \frac{S_v}{2.25\sqrt{d_{50}}} \right)^{3.5} (1 - 1.25 S_v) \right] \tag{21}$$

where d_{50} is the medium diameter of a group of sediment.

2.5. Bedload sediment transport rate

Bedload transport rate is an important parameter that can be computed as following (Dou, *et al.* 1995):

$$g_{b,L} = K_0 \frac{\gamma_s U' \overline{U}^3}{\frac{\gamma_s - \gamma}{\gamma} g \omega_L C_0^2} \tag{22}$$

where K_0=0.001; $C_0 = h^{1/6}/(ng^{1/2})$; $U' = \begin{cases} \overline{U} - U_c, & \overline{U} > U_c \\ 0, & \overline{U} \le U_c \end{cases}$; U_c = the incipient velocity of sediment, which can be calculated by:

$$U_c = 0.265 \ln\left(\frac{11h}{\Delta}\right) \sqrt{\frac{\gamma_s - \gamma}{\gamma} gd + 0.19 \frac{\varepsilon_k + gh\delta}{d_{b50}}} \tag{23}$$

in which d_{b50} =the medium bedload diameter; $\varepsilon_k = 2.56 \times 10^{-6} m^3/s^2$; $\delta = 0.12 \times 10^{-6} m$; Δ = roughness height of rive bed and can be determined as:

$$\Delta = \begin{cases} 0.5mm, & D_{50} \le 0.5mm, \\ D_{50}, & D_{50} > 0.5mm. \end{cases} \tag{24}$$

2.6. Recovering saturation coefficient

Recovering saturation coefficient in (6) and (7) can be evaluated by (Wei *et al.* 1997)

$$\alpha_L = \begin{cases} 0.001/\omega_L^{0.3}, & S_L \geq S_L^* \\ 0.001/\omega_L^{0.7}, & S_L < S_L^* \end{cases} \tag{25}$$

3. Numerical methods

3.1. Discretization of the governing equations

The general governing equation (10) is discretized with finite volume method (FVM) (Versteeg and Malalasekera 1995). The computational domain is rectangular in the BFC system and can be easily divided into a series of small rectangles, as shown in Figure 1. Collocated grid system is adopted in this study. In order to avoid the checkerboard pressure difference, momentum interpolation method (Rhie and Chow, 1983) is used. The representative control volume is ΔV and its centre is node *P*. The east, west, south and north faces of the control volume are *e*, *w*, *s* and *n*, respectively. The east, west, south and north neighbor nodes of P are *E*, *W*, *S* and *N*, respectively. Integrating Eq. (10) over the control volume ΔV yields:

$$\begin{aligned} &\int_{\Delta V} \frac{\partial}{\partial t}(h\Phi)dV + \int_{\Delta V} \frac{1}{J}\frac{\partial}{\partial \xi}(hU\Phi)dV + \int_{\Delta V} \frac{1}{J}\frac{\partial}{\partial \eta}(hV\Phi)dV \\ &= \int_{\Delta V} \frac{1}{J}\frac{\partial}{\partial \xi}(\frac{\alpha h\Gamma_\Phi}{J}\frac{\partial \Phi}{\partial \xi})dV + \int_{\Delta V} \frac{1}{J}\frac{\partial}{\partial \eta}(\frac{\gamma h\Gamma_\Phi}{J}\frac{\partial \Phi}{\partial \eta})dV + \int_{\Delta V} S_\Phi(\xi,\eta)dV \end{aligned} \tag{26}$$

The first term (i.e. unsteady term, represented by I_t) on the left hand side is discretized by the first order implicit scheme:

$$I_t = \frac{h_P\Phi_P - h_P^*\Phi_P^*}{\Delta t} J_P \Delta\xi\Delta\eta \tag{27}$$

where $\Delta t, \Delta\xi, \Delta\eta$ are time step, spatial steps in ξ and η directions, respectively. Subscript *

represents the variable of the last time step.

The second and third terms (i.e. convective terms, represented by I_C) on the left hand side are discretized using an improved QUICK scheme developed by Hayase, *et al.* (1992). In this scheme, a deferred correction method presented by Khosla and Rubin (1974) is used to improve the QUICK scheme.

$$I_C = E_e - E_w + E_n - E_s \tag{28}$$

where

$$E_e = [|F_e,0|]\left(\Phi_P + \frac{1}{8}(3\Phi_E - 2\Phi_P - \Phi_W)^*\right) + [|-F_e,0|]\left(\Phi_E + \frac{1}{8}(3\Phi_P - 2\Phi_E - \Phi_{EE})^*\right) \tag{29}$$

$$E_w = [|F_w,0|]\left(\Phi_W + \frac{1}{8}(3\Phi_P - 2\Phi_W - \Phi_{WW})^*\right) + [|-F_w,0|]\left(\Phi_E + \frac{1}{8}(3\Phi_W - 2\Phi_P - \Phi_E)^*\right) \tag{30}$$

$$E_n = [|F_n,0|]\left(\Phi_P + \frac{1}{8}(3\Phi_N - 2\Phi_P - \Phi_S)^*\right) + [|-F_n,0|]\left(\Phi_N + \frac{1}{8}(3\Phi_P - 2\Phi_N - \Phi_{NN})^*\right) \tag{31}$$

$$E_s = [|F_s,0|]\left(\Phi_S + \frac{1}{8}(3\Phi_P - 2\Phi_S - \Phi_{SS})^*\right) + [|-F_s,0|]\left(\Phi_P + \frac{1}{8}(3\Phi_S - 2\Phi_P - \Phi_N)^*\right) \tag{32}$$

In which $[|F_e,0|] = max(F_e,0)$, $F_e = (hU\Delta\eta)_e$, $F_n = (hV\Delta\xi)_n$.

As a result, the scheme has not only the third order accuracy, but is also diagonally dominant and can be easily programmed.

The first and second terms on the right hand side (i.e. diffusion terms, represented by I_D) are discretized using the second order central difference scheme.

$$I_D = D_e(\Phi_E - \Phi_P) - D_w(\Phi_P - \Phi_W) + D_n(\Phi_N - \Phi_P) - D_s(\Phi_P - \Phi_S) \tag{33}$$

where

$$D_e = \left(\frac{\alpha \Gamma_\Phi h}{J}\right)_e \frac{\Delta\eta}{(\delta\xi)_e}, D_n = \left(\frac{\gamma \Gamma_\Phi h}{J}\right)_n \frac{\Delta\xi}{(\delta\eta)_n}.$$

The last term on the right hand side (the source term, represented by I_S) can be dealt with using the following local linear method:

$$I_{S_\Phi} = I_{S_{\Phi C}} + I_{S_{\Phi P}} \Phi_P \tag{34}$$

where $I_{S_{\Phi P}} \le 0$. As for momentum equations, the source terms are as following:

$$I_{S_{uC}} = -\Delta\xi\Delta\eta\left[gh(z_\xi y_\eta - z_\eta y_\xi) + \frac{\partial}{\partial\xi}\left(\frac{\beta\Gamma_u h}{J}\frac{\partial u}{\partial\eta}\right) + \frac{\partial}{\partial\eta}\left(\frac{\beta\Gamma_u h}{J}\frac{\partial u}{\partial\xi}\right) + \frac{1}{J}\frac{u\sqrt{\gamma}}{\sqrt{u^2+v^2}}\frac{\partial}{\partial\eta}\left(|\bar{u}|\bar{u}\phi\right)\right]$$

$$I_{S_{vC}} = -\Delta\xi\Delta\eta\left[gh(-z_\xi x_\eta + z_\eta x_\xi) + \frac{\partial}{\partial\xi}\left(\frac{\beta\Gamma_v h}{J}\frac{\partial v}{\partial\eta}\right) + \frac{\partial}{\partial\eta}\left(\frac{\beta\Gamma_v h}{J}\frac{\partial v}{\partial\xi}\right) + \frac{1}{J}\frac{v\sqrt{\gamma}}{\sqrt{u^2+v^2}}\frac{\partial}{\partial\eta}\left(|\bar{u}|\bar{u}\phi\right)\right]$$

$$I_{S_{uP}} = I_{S_{vP}} = -\frac{gn^2\sqrt{u^2+v^2}}{h^{1/3}} J_P \Delta\xi\Delta\eta.$$

The discretized equation of the general governing equation (10) using the above discretized scheme is as following:

$$a_P\Phi_P = a_E\Phi_E + a_W\Phi_W + a_N\Phi_N + a_S\Phi_S + I_{S_{\Phi C}} + S^*_{ad} \tag{35}$$

where

$$a_E = D_e + [|-F_e, 0|], a_W = D_w + [|F_w, 0|], \quad a_N = D_n + [|-F_n, 0|], a_S = D_s + [|F_s, 0|],$$

$$a_P = a_E + a_W + a_N + a_S + F_e - F_w + F_n - F_s + a^*_P - I_{S_{\Phi P}}, b = a^*_P\Phi^*_P + I_{S_{\Phi C}},$$

$$a^*_P = \frac{h^*_P}{\Delta t} J_P \Delta\xi\Delta\eta, \quad S^*_{ad} = (S^*_{ad})_e + (S^*_{ad})_w + (S^*_{ad})_n + (S^*_{ad})_s,$$

$$(S^*_{ad})_e = \frac{1}{8}(3\Phi_E - 2\Phi_P - \Phi_W)^*[|F_e, 0|] + \frac{1}{8}(3\Phi_P - 2\Phi_E - \Phi_{EE})^*[|-F_e, 0|],$$

$$(S^*_{ad})_w = \frac{1}{8}(3\Phi_P - 2\Phi_W - \Phi_{WW})^*[|F_w, 0|] + \frac{1}{8}(3\Phi_W - 2\Phi_P - \Phi_E)^*[|-F_w, 0|],$$

$$(S_{ad}^{*})_n = \frac{1}{8}(3\Phi_N - 2\Phi_P - \Phi_S)^{*}[|F_n, 0|] + \frac{1}{8}(3\Phi_P - 2\Phi_N - \Phi_{NN})^{*}[|-F_n, 0|],$$

$$(S_{ad}^{*})_s = \frac{1}{8}(3\Phi_P - 2\Phi_S - \Phi_{SS})^{*}[|F_s, 0|] + \frac{1}{8}(3\Phi_S - 2\Phi_P - \Phi_N)^{*}[|-F_s, 0|].$$

Collocated grids SIMPLEC algorithm in body fitted coordinate system (Van Doormaal and Raithby 1984) is used to solve the coupled problem of water level and velocities. The discretized equations are five-diagonal, which can be solved using alternative direction tridiagonal matrix algorithm (TDMA) (Versteeg and Malalasekera 1995).

3.2. Semi-coupled scheme for sediment model

In this study, a semi-coupled scheme is developed by combining the advantages of coupled and decoupled schemes. In the process of long time simulation of sediment transport when river bed changes slowly, the bed elevation change each time step has minimal impacts on flow field, therefore, it is unnecessary to update the hydraulic elements each time step. Thus, in order to reduce the computational cost, the hydraulic module runs intermittently while the sediment module keeps running all the time. In the semi-coupled scheme, after the sediment module starts to run, the hydraulic module will stop running for a certain number of time steps (for example, 1000-5000 time steps), then it will run again. After running for certain time steps (such as 60-120 time steps) to update the hydraulic elements, it will then stop running. The process is repeated until the required accuracy is reached.

Let *t* be simulating time, *t0_flow* the initial simulation time for the flow module, *t1_flow* the flow module working time each time, *t2_flow* the time interval between two adjacent times when flow

298 module is started, *t_max* the whole simulation time. The procedure of this semi-coupled scheme is
299 detailed as following:
300
301 ***Algorithm of semi-coupled scheme:***
302 Step 1. If t≤t0_flow, only the flow module is running；
303 Step 2. If t0_flow< t<t_max, the sediment module is running.
304 Step 3. If t0_flow< t<t_max, and mod (t, t2_flow)<t1_flow, the flow and sediment modules are
305 running together； otherwise, only the sediment module is running.
306 Step 4. If t>t_max, stop.
307 where mod is a function which means modulus and mod (t, t2_flow) is the remainder when t is
308 divided by t2_flow. In this study, time step dt=12s, t0_flow=5h, t1_flow=1h, t2_flow=12h.
309 Numerical experiments indicate that the computational time of the semi-coupled scheme is about
310 60% of the coupled scheme.
311
312 ***3.3. Boundary and initial conditions***
313 We choose two adjacent field measurements to verify the sediment model. The field measurements
314 were conducted on December 6, 2008 and on July 17, 2009, respectively. The time interval
315 between the two measurements is 203 days. Water discharge and sediment concentration are given
316 at the inlet based on values interpolated by field data measured on December 6, 2008 and on July
317 17, 2009. The turbulence kinetic energy (k) and its dissipation rate (ε) at the inlet are calculated
318 using empirical formulae (Rodi 1993). On the water outlet boundary, water level is specified based
319 on the values by interpolating the field data measured on December 6, 2008 and on July 17, 2009.

Other variables are dealt with using the fully developed condition. On the wall boundary, no-slip boundary condition is applied. The velocity parallel to the river bank at the first cell is estimated using standard wall function (Guo, et al. 2008).

In order to study the flow and sediment transport in the studied reach, four cases are used based on discharge and sediment concentration at the inlet. The boundary conditions of the four cases are presented in Table 1. Case 1 is set according to the field measured data on December 6, 2008, while Case 2 is set according to the data measured on July 17, 2009. Case 3 and Case 4 are set according to the hydrological data in the past years. Cases 1 and 4 represents the hydraulic conditions of dry and flood seasons, respectively, while Cases 2 and 3 represents hydraulic condition of wet season.

The initial values are based on field measured data on December 6, 2008, including the position of cross-sections, water level, maximum water depth, average water depth, river width, average velocity of 14 cross-sections (see Table 2). The initial water level at each grid is set as the same as the water level at the outlet. u, v and S_L at each grid are set as zero, except for the grids at the inlet. However, k and ε can not be set as zero, otherwise, the simulation process will stop unexpected or be unstable. In the simulations, the initial values of k and ε are set as 0.1 m^2/s^2 and 0.0001 m^2/s^2, respectively, based on the authors' experience.

The suspended and bedload sediment at the inlet section is divided into three groups with the medium diameter being 0.0249 *mm* and 10 *mm*, respectively. The representative diameters and

related percentage for both the suspended and bedload sediment are listed in Table 3. The bed material is divided into six groups, whose representative diameters and their percent content are also presented in Table 3. The initial percentage contents of the suspended and bedload are set as the same as the values at the inlet. Some representative diameters of the initial bed material of the whole reach are: d_{50} =10 mm, d_m =15.5 mm, $d_{25}=1$ mm, $d_{35}=4$ mm, $d_{75}=20$ mm, $d_{90}=70$ mm and $d_{95}=100$ mm, where d_m = the mean diameter, d_a = the sediment diameter that a% is less than that in the size gradation curve (a=25, 35,50,75,90,95).

3.4. Mesh generation

In the computational domain, along longitudinal direction (ξ-direction), 131 grids are assigned, while along transverse direction (η-direction), 31 grids are set. Poisson equation method is used to make body-fitted coordinate transformation and grid generation (Versteeg and Malalasekera 1995). The total number of grids and cells are 4991 and 4800, respectively. To better fit the complex boundary, non-uniform meshes with arbitrarily spatially dependent size were used. This allows for locally refining the concerned regions (e.g. near bends) with small meshes and has the advantage of flexibly assigning meshes in the computational domain. Along transverse direction, there are 30 cells, in which 5 non-uniform cells near left bank and near right bank, respectively. The gird length of the 5 cells near bank increases from bank to interior. Figure 2 shows the mesh distribution near banks and bends.

4. Results and discussions

4.1. Description of the computational domain and numerical simulation

The Shapotou Reservoir in the Yellow River is located in Ningxia Hui Autonomous Region in China. The studied reach is about 13.4km long, as shown in Figure 3. Twenty cross-sections (e.g. SH1-SH15, SHJ1-SHJ5) are assigned in the studied reach, in which SH15 is the inlet, and SH1 is the outlet. The studied reach consists of five bends: Bend A (from SH15 to SH13), Bend B (from SH13 to SH11), Bend C (from SH11 to SH7), Bend D (from SH7 to SH2) and Bend E (from SH2 to SH1). Bends A and B are near the exit of the Heishan Gorge, where the river is deep and narrow, and the current is rapid. The averaged water width at bend A and Bend B is about 135m with the normal water level gradient being about 0.03%. Bends C, D and E are near the Shapotou Dam, where the river is wide and shallow (the averaged water width is about 300 m), and the current is slow. The normal water level gradient is about 0.006% .

In the simulation, the semi-coupled scheme in the 2D depth averaged RNG k-ε sediment model is applied. The software of Matlab 7.1 is used to program, and the numerical simulation is performed on an IBM work station. The CPU of the work station is two cores Intel ® Xeon 2.0G Hz; the memory is 4.0GB; the operation system is Ghost-Server2003 SP2. Typical numerical simulation takes about 16 days.

4.2. Sediment setting velocity

The sediment setting velocities of the six representative groups in the studied reach are calculated by (19) and modified by (20), as listed in Table 4.

386 The sediment setting velocity is affected by the sediment concentration. Here we assume that the
387 sediment concentration is S=10kg/m^3 and the sediment concentration by volume is
388 $S_v=S/\rho_s$=0.0038 (ρ_s = density of sediment=2650kg/m^3). It is seen that the same sediment
389 concentration has different influence for the setting velocity of various grain size groups. The
390 correction rate is bigger for fine sediment than that for coarse sediment. In other words, sediment
391 concentration has larger effect on fine sediment than on the coarse one.
392
393 ***4.3. Suspended sediment carrying capacity***
394 The suspended sediment carrying capacity is calculated using (16) and (17) for different group
395 sediment carrying capacity. Because the numerical results about suspended sediment carrying
396 capacity of the four cases are similar, only the result under the condition of Case 2 is presented in
397 this paper. Figure 4 shows the distribution of sediment concentration, total and group suspended
398 sediment carrying capacities along the centerline of the studied river reach. As shown in Figure 4,
399 both total and group sediment carrying capacities decrease along the way. It can also be found that
400 the carrying capacity of the second sediment group is the largest among the three sediment groups,
401 while the carrying capacity of the third sediment group is the smallest, which is consistent with the
402 sediment concentration of the three groups at the inlet.
403
404 ***4.4. Bedload sediment transport rate***
405 In this study, four different methods are applied to calculate bedload sediment transport. The first
406 method (Method I) is to calculate group bedload transport rate by (22), then summing them to
407 obtain the total transport rate. The second method (Method II) is to calculate ω by (20) and (21),

where the representative sediment diameter (d) is chosen as d_{35}; then replacing ω_L with ω in (21) to calculate the total bedload sediment transport rate. The third method (Method III) is the same as Method II, except that the representative sediment diameter is d_m. The fourth method (Method IV) is the same as Method II, except that d_{50} is chosen as the representative sediment diameter.

From Table 5, it can be seen that the bedload transport rates calculated using the four methods are different. Generally speaking, for non-uniform bedload sediment, it would be more accurate to divide bedload sediment into several groups when computing its transport rate. Therefore, the result calculated using Method I is the most reliable. The result calculated by Method II is closer to the result of Method I, indicating that the transport rate of non-uniform bedload sediments can be calculated using the formula for computing the transport rate of uniform bedload sediments when the representative sediment diameter is chosen as d_{35} for the flow and sediment conditions investigated here This result is consistent with the conclusion of Einstein (Zhang, 1988).

4.5. Comparison between measured and calculated velocities

Figure 5 shows the comparison of the simulated and field measured (on July 16 2009) depth averaged velocities on three selected cross-sections, i.e. SH7, SH5, SHJ2, which are near the inlet, apex, and outlet of Bend D, respectively. Figure 5(1) also shows the comparison of the depth averaged velocities calculated using two methods: Simulation 1 and Simulation 2. In Simulation 1, the circulation flow is not taken into account, while this has been taken into account in Simulation 2. It is seen that the simulated velocity using the second approach is better compared to the

measured data than that using the first method, indicating that the modified plane 2D RNG *k-ε* model is capable of simulating the effect of the circulation flow in natural rivers. In general, good agreements between simulated and field measured velocities at three cross sections are obtained.

4.6. Comparison between measured and calculated river bed deformation

Figure 6 is the plot of the simulated and field measured (on July 17 2009) bed elevation along the longitudinal direction. It is seen that the simulated bed elevation is in good agreement with the measured data. From SH11 to SH9, the river bed is scoured, while from SHJ5 to SH2, the river bed is deposited. The deposit thickness varies significantly from SH2 to SH5 with the largest deposition taking place in SH2 (where the average deposit thickness is over 1 m), while little deposit takes place at SH5 (where the average deposit thickness is only about 0.01 m).

In Figure 7, the measured and the simulated bed elevations at three typical cross sections are plotted. The three cross sections are SH10, SHJ5 and SH7, which are near the inlet, the bend apex, and the outlet of Bend C, respectively. It is seen from Figure 7 that the simulated bed elevation agrees well with the measured data on these cross sections, indicating that the 2D depth averaged RNG k-ε sediment model can reasonably simulate the bed deformation in the studied reach. The bed on SH10 is scoured as a whole except some small areas near the river banks. The bed near the left bank of SHJ5 and SH7 is deposited and the bed near the right bank of the two cross-sections is scoured. Because the left bank is the convex bank，while the right bank is the concave bank in Bend C, the above phenomenon is in consistence with the general rule of sediment transport in a bend.

4.7. Suspended sediment transport

Figure 8 shows the distribution of suspended sediment concentration along the centerline of the studied reach under the condition of Case 2 with the sediment concentration at the inlet being set as 0.51, 3.53, 10 and 20 kg/m^3, respectively. From Figure 8, it is seen that the suspended sediment concentration in the studied reach increases with increasing the suspended sediment concentration at the inlet. As the river of the studied reach becomes wider and shallower as the flow moves downstream, the flow becomes slower and the sediment carrying capacity becomes weaker accordingly along the way, leading to the decrease of the suspended sediment concentration along the way.

4.8. The effect of discharge on river bed deformation

In order to investigate the effect of the discharge at the inlet on the bed deformation, numerical simulations were conducted for four cases. The conditions of the four cases are shown in Table 1 except that the sediment concentration at the inlet is set as 3.53kg/m^3. Figure 9 shows the simulated bed elevation after 10 days development for all four cases. The bed is deposited near the inlet for Cases 1 and 2, while the bed is scoured near the inlet under the condition of Cases 3 and 4. The reason is that the average velocities for the Cases 1 and 2 are small, and the suspended sediment capacities are smaller than the sediment concentration. As a result, the bed is deposited near the inlet. However, after flow moves a certain distance, a balance between deposition and scour is reached. The position of balance is about 9.5km from the inlet for Case 1, and it is near SH5; while for Case 2, it is about 10.5km from the inlet and near SH4. The discharges and average

474 velocities of the Cases 3 and 4 are larger, and the suspended sediment capacities of the two cases
475 are larger than sediment concentration. Therefore, the bed is scoured near the inlet. Similar to
476 Cases 1 and 2, a balance between deposition and scour is reached after the flow moves a certain
477 distance away from the inlet. For Case 3, the position is about 4.5km from the inlet and near SH10;
478 while for Case 4, the position is about 6km from the inlet and near SHJ5. From above analysis, it
479 can be concluded that the discharge at the inlet has significant influence on the bed deformation
480 near the inlet. However, after the flow moves a certain distance, the influence becomes weaker and
481 weaker.
482
483 ***4.9. River bed deformation caused by bedload sediment***
484 Though the bed deformation is mainly caused by the suspended sediment transport, the bedload
485 sediment transport can also have significant effect on the bed deformation for some certain
486 situations. To investigate the effect of bedload sediment transport on the river bed deformation, the
487 numerical simulation is conducted for four cases with the same suspended sediment concentration
488 at the inlet being 3.53kg/m^3. Figure 10 shows the percentage of the absolute thickness deposited or
489 scoured by suspended and bedload sediments for four typical cases after 10 days development,
490 respectively. It can be seen that the thicknesses deposited or scoured due to the suspended or
491 bedload sediment transport is quite different. In Cases 1 and 2, the percentage of bed deformation
492 caused by bedload sediment is less than 1%, which is negligible. In Case 3, the percentage is less
493 than 3% and is still very small and can be neglected. In Case 4, however, the percentage is about
494 10%, which can not be neglected. Therefore, it can be concluded that the bed deformation caused
495 by bedload sediment can be neglected when the discharge at the inlet is small (less than 1500m^3/s

496 in this study). When the discharge at the inlet is larger (more than 2000m^3/s in this study),
497 however, the bed deformation caused by bedload sediment reaches a certain level and has to be
498 taken into account. .
499
500 ***4.10. The variation of effective bed material granularity***
501 Bed material becomes finer or coarser when the bed is deposited or scoured and it is worth of
502 investigating. Because the simulated results for four cases are similar, only the numerical result of
503 Case 4 is presented and discussed in this paper. Under the condition of Case 4, numerical
504 simulations were conducted for the sediment concentration at the inlet (S_{in}) being 0.51kg/m^3 and
505 10kg/m^3, respectively.
506
507 Figure 11 shows the variation of effective bed material granularity along the river flow direction
508 after 20 days. In Figure 11, the axis x is the distance from the inlet, and the axis y is the percentage
509 of each group effective bed materials. The percentage of the initial bed material for the six groups
510 is 0.2%, 3.8%, 17.9%, 12.7%, 36.5%, 28.9%, respectively, as shown by the dash line in Figure 11.
511
512 When S_{in} = 0.51kg/m^3, the river bed is scoured as a whole and the bed material size gradation is
513 changed after 20 days' scouring. In Figure 11(a), it is seen that the percentage of the first three
514 groups (Groups 1-3) of bed material decreased compared with the initial value, especially for
515 Groups 2 and 3. The decreasing tendency becomes weaker with the distance and reaches the
516 minimum at the distance from the inlet. Meanwhile, the percentage of the last three groups
517 (Groups 4-6) of bed material increased compared with the initial value. The increasing tendency

also becomes weaker with the distance and reaches the minimum at the distance of 8.5km from the inlet (near SH6). And after SH6, the bed material granularity is almost not changed for all of the 6 groups. This means that bed becomes coarser when the bed is scouring. However, after SH6, the sediment concentration at the inlet has little influence to the bed deformation and variation of bed material granularity, as shown by Figure 9 and Figure 11.

When S_{in}=10kg/m^3, the situation is different and complicated. As shown in Figure 11(b), the bed material percentage of Groups 1-3 increases, while the percentage of Groups 4-6 decrease as a whole compared with the initial value. In Figure 11(b), it can also be found that the percentage of the first three groups of the bed material increases with the distance and reaches the maximum near SH6. The percentage of these groups then decreases with the distance. To the contrary, the last three groups of the bed material decreases with the distance and reaches the minimum at about 8.5 km from the inlet and increases again to the outlet. This means that the river bed becomes finer compared with the initial value when it is deposited. Similar to the condition when S_{in}=0.51 kg/m^3, after SH6, the sediment concentration at the inlet has little influence to the bed deformation and variation of bed material granularity.

5. Conclusions

In this study, a 2D depth averaged RNG k-ε sediment model including the effects of secondary currents is developed, which considers the effects of the non-uniform suspended and bedload sediment transport on the bed deformation. In the model, the variation of effective bed material size distribution is included. A semi-coupled scheme is developed by combining the coupled and

decoupled schemes to improve the accuracy of the numerical simulation (compared with the decoupled scheme) and save computational time (compared with the coupled algorithms). Numerical simulations have been performed for four typical cases to investigate the sediment transport and bed deformation in the upper reach of the Yellow River. Comparison between the numerical results and field measurements indicates that the 2D depth averaged RNG k-ε sediment model can reasonably simulate the sediment transport and the resultant bed deformation of rivers with continuous bends. River bed deformation induced by suspended and bedload sediment transport has been investigated. It is found that the bed deformation caused by bedload sediment transport can be neglected when the discharge at the inlet is small (less than 1500m^3/s in this study). The results also show that the discharge at the inlet has significant effect on the bed deformation near the inlet. The influence, however, becomes weaker as the flow moves downstream.

The variation of effective bed material granularity has been examined. It is concluded that the bed material granularity becomes finer when the bed is deposited. When the bed is scoured, the bed material granularity becomes coarser. The bed material granularity becomes finer along the way in the studied reach no matter it is deposited or scoured. The sediment concentration at the inlet has significant influence for bed material granularity near the inlet. However, the influence becomes weaker with the distance from the inlet.

6. Acknowledgements

The authors acknowledge with thanks the following institutes for assisting this study: Ningmeng

562 Hydrographic & Water Resource Office of Yellow River Water Conservancy Committee of China,
563 and Ningxia Shapotou Hydraulic Power Plant of China. Constructive comments and suggestions
564 from the Editor and reviewers have greatly improved the quality of the paper.
565

566 **7. References**

567 Dou, G.R., Dong, F.W., Dou, X.P., Li, T.L., 1995. Mathematical modeling of sediment transport in
568 estuaries and coastal regions. *Science in China(Series A)*, 38 (10):1251-1260.

569 Duan, J.G., Nanda, S.K., 2006. Two-dimensional depth-averaged model simulation of suspended
570 sediment concentration distribution in a groyne field. *Journal of Hydrology*, 327, 426-437.

571 Duan, J.G., Julien, P.Y., 2010. Numerical simulation of meandering evolution. *Journal of*
572 *Hydrology*, 391: 34-46.

573 Falconer, R.A. 1992. Flow and water quality modelling in coastal and inland water. *J. Hydraul.*
574 *Res.*, 30, 437-452.

575 Guo, Y.K., Wang, P.Y., Zhou, H., 2007. Numerical modelling of the flow past irregularities in a
576 pressure conduit, *ASCE J. Hydr. Eng.*, 133(6): 698-702.

577 Guo, Y.K., Zhang, L.X., Shen, Y.M., Zhang, J.S., 2008. Modeling study of free overfall in a
578 rectangular channel with strip roughness, *ASCE J. Hydr. Eng.*, 134(5): 664–667.

579 Guo, Y.K., Wu, X.G., Pan, C.H., Zhang, J., 2012. Numerical Simulation of the Tidal Flow and
580 Suspended Sediment Transport in the Qiantang Estuary, *ASCE Journal of Waterway, Port, Coastal*
581 *and Ocean Engineering*, 138: 192-203.

582 Hayase, T., Humphrey, J.A.C., Greif, G.., 1992. A consistently formulated QUICK scheme for fast
583 and stable convergence using finite volume iterative calculation proceeding. *J. Comput. Phys.*,

584 98:108-118.

585 Hung, M.C., Hsieh, T,Y,, Wu, C.H., Yang, J.C., 2009. Two-Dimensional nonequilibrium
586 noncohesive and cohesive sediment transport model. *J. Hydr. Eng.(ASCE)*, 135(5) : 369-382

587 Jing, H.F., Guo, Y.K., Li, C.G., Zhang, J.S., 2009. Three-dimensional numerical simulation of
588 compound meandering open channel flow by the Reynolds stress model. *Int. J. Numer. Mech.*
589 *Fluids*, 59, 927-943.

590 Jing, H.F., Li, C.G., Guo, Y.K., Xu, W.L., 2011. Numerical simulation of turbulent flows in
591 trapezoidal meandering compound open channels. *Int. J. Numer. Mech. Fluids*, 65, 1071-1083.

592 Khosla, P.K., Rubin, S.G., 1974. A diagonally dominant second order accurate implicit scheme.
593 *Computer & Fluids*, 2:207-209.

594 Li, S.S., Millar, R.G., 2011. A two-dimensional morphodynamic model of gravel-bed river with
595 floodplain vegetation. *Earth Surface Process & Landforms*, 36(2): 190-202.

596 Lien, H.C., Hsieh, T.Y., Yang, J.C., Yeh, K.C., 1999. Bend-flow simulation using 2D
597 depth-averaged model. *ASCE J. Hydr. Eng.*, 125, 1097-1108.

598 Nagata, N., Hosoda, T., Muramoto, Y., 2000. Numerical analysis of river channel processes with
599 bank erosion. *ASCE J. Hydr. Eng.*, 126 (4): 243 -252.

600 Rhie, C.M., Chow, W.L., 1983. A numerical study of the turbulent flow past an isolated airfoil
601 with trailing edge separation. *AAIA J.*, 21:1525-1532.

602 Rodi, W., 1993. *Turbulence models and their application in hydraulics: A state-of-the-art review*,
603 *3rd Ed.*, Balkema, Rotterdam, the Netherlands.

604 Serrano-Pacheco, A., Murillo, J., Garcia-Navarro, P., 2012. Finite volumes for 2D shallow-water
605 flow with bed-load transport on unstructured grids, *Journal of Hydraulic Research*, 50(2):

154-163.

Van Doormaal, J.P., Raithby, G.D., 1984. Enhancement of SIMPLE method for predicting incompressible fluid flows. *Numer. Heat Transfer*, 7(2): 147-163.

Versteeg, H.K., Malalasekera, W., 1995. *An introduction to computational fluid dynamics.* Addison Wesley Longman Limited, England.

Wei, Z.L., Zhao, L.K., Fu, X.P., 1997. Research on mathematical model for sediment in Yellow River, *J. Wuhan University of Hydro. & Electric Eng*., 30(5):21-25.

Yakhot, V., Orzag, S.A., 1986. Renomalization group analysis of turbulence: basic theory. *J. Scient Comput.*, 1, 3-11.

Zhang, H.W., Zhang, Q., 1992. Formula of Sediment Carrying Capacity of the Yellow River . *Yellow River*, (11):6-9.

Zhang, R.J., 1988. *River Sediment Dynamics(the second edition)*. Beijing: Water Conserversy and Hydropower of China.

Captions of figures:

Figure 1 The grid and control volume of finite volume method

Figure 2 Meshes distribution near banks and bends

Figure 3 Plane view of Shapotou reservoir(The flow is in from SH15 and out from SH1, and the direction of axis x is consistent with the east)

Figure 4 The distribution of total and group suspended sediment capacities(Case 2)

Figure 5 Comparison of simulated and measured depth averaged velocities on three typical cross-sections

Figure 6 Comparison of simulated and measured bed elevation along the longitudinal direction

Figure 7 Comparison of the measured and the simulated bed elevations on three typical cross sections:（1）SH10（2）SHJ5（3）SH7

Figure 8 Distribution of suspended sediment concentration along the centerline of the studied reach under the condition of Case 2

Figure 9 Comparison of the simulated bed deformations among the four cases with the same sediment concentration（3.53kg/m^3）at the inlet

Figure 10 Percentage of bed deformation caused by bedload sediments in four cases

Figure 11 The variation of effective bed material composition after 20 days:

(1) (a) S_{in}=0.51kg/m^3 (b) S_{in}=10kg/m^3

639 Table 1 Boundary conditions of four cases

Cases	Inlet					Outlet
	Q（m^3/s）	U（m/s）	S（kg/m^3）	k(m^2/s^2)	ε(m^2/s^3)	z(m)
Case 1	513.50	1.0398	0.51	0.0121	0.0005	1239.68
Case 2	930.00	1.5405	3.53	0.0269	0.0013	1240.65
Case 3	1500.00	1.8098	10	0.0378	0.0016	1241.50
Case 4	2000.00	2.0579	20	0.0492	0.0020	1242.00

640

641

642 Table 2. Some data measured on December 6, 2008

Cross section No.	Distance from the inlet /km	Water level /m	Maximum water depth /m	Average water depth/m	River width /m	Average velocity /m/s
SH2	12.52	1240.51	8.58	6.19	212.10	0.35
SH3	11.71	1240.53	6.10	5.31	269.50	0.31
SHJ2	11.26	1240.54	5.78	5.40	267.50	0.33
SH4	10.58	1240.58	6.70	5.47	215.50	0.49
SHJ3	10.14	1240.76	8.43	5.28	214.90	0.52
SH5	9.68	1240.79	8.47	5.07	228.00	0.56
SH6	8.70	1240.82	7.14	4.47	295.40	0.44
SHJ4	8.20	1240.86	6.23	4.69	259.30	0.49
SH7	7.60	1240.88	6.49	4.75	234.20	0.38
SH8	6.75	1240.90	7.34	5.44	221.70	0.35
SHJ5	6.25	1240.91	6.04	4.72	245.90	0.53
SH9	5.55	1241.02	6.45	4.84	175.90	0.54
SH10	4.69	1241.27	13.68	7.67	115.00	0.44
SH11	3.70	1241.38	6.29	4.65	155.90	0.81

643

644

645

646 Table 3 The initial percent content of bed materials, suspended sediment and bedload

group	1	2	3	4	5	6
diameters /mm	0.01	0.05	0.25	2	10	40
Bed materials /%	0.2	3.8	17.9	12.7	36.5	28.9
Suspended sediment /%	38	53	9			
Bedload /%				38.3	31.3	30.4

647

648

649

650 Table 4 Sediment group setting velocity of six groups

Sediment grain size /mm	Single setting velocity (cm / s)	Group setting velocity (cm / s)	Correction rate (%)
0.01	0.0062	0.0059	4.92
0.05	0.1570	0.1522	3.14
0.25	1.6142	1.5877	1.69
2	5.8798	5.8277	0.91
10	13.3038	13.2164	0.67
40	26.6075	26.4575	0.58

651

652

653 Table 5 Bedload sediment transport rate at the centerline of some cross sections calculated by
654 four methods under the condition of Case 2 (unit: kg/ms)

Cross sections	Method I	Method II	Method III	Method IV
SH1	0.0018	0.0023	0	0
SH2	0.0006	0.0003	0	0
SHJ2	0.0013	0.0014	0	0
SHJ3	0.0003	0	0	0
SH6	0.001	0.001	0	0
SH7	0.0033	0.0046	0	0
SHJ5	0.0028	0.0037	0	0
SH10	0.0111	0.013	0.0001	0.0034
SH12	0.0499	0.0523	0.0128	0.0228
SH14	0.0415	0.0439	0.0099	0.0184

655

656

657

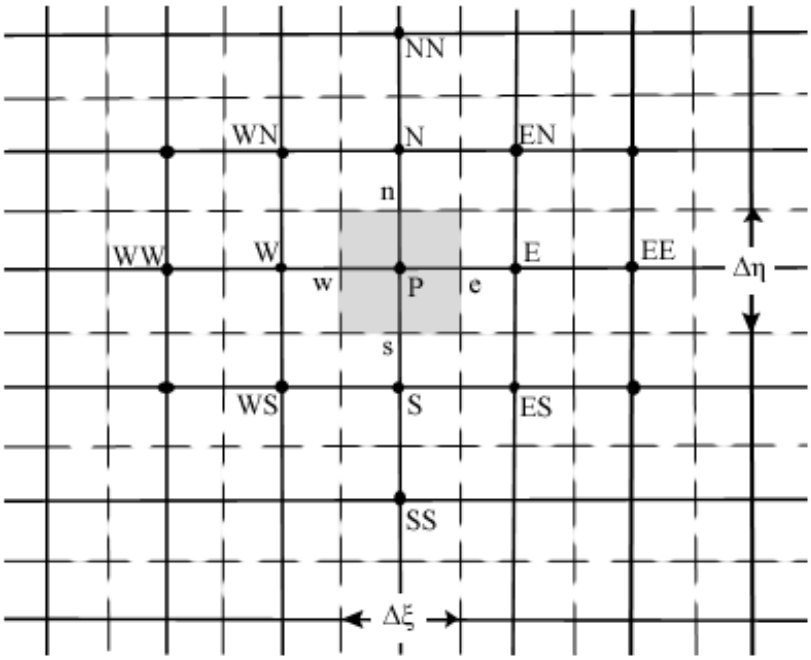

Figure 1 The grid and control volume of finite volume method

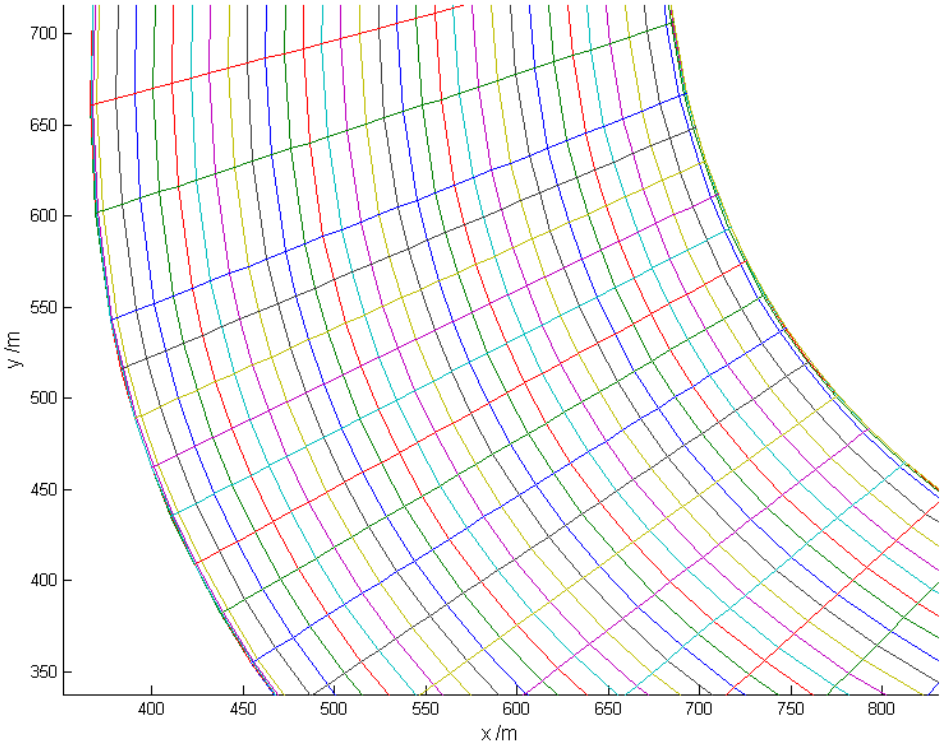

Figure 2 Meshes distribution near banks and bends

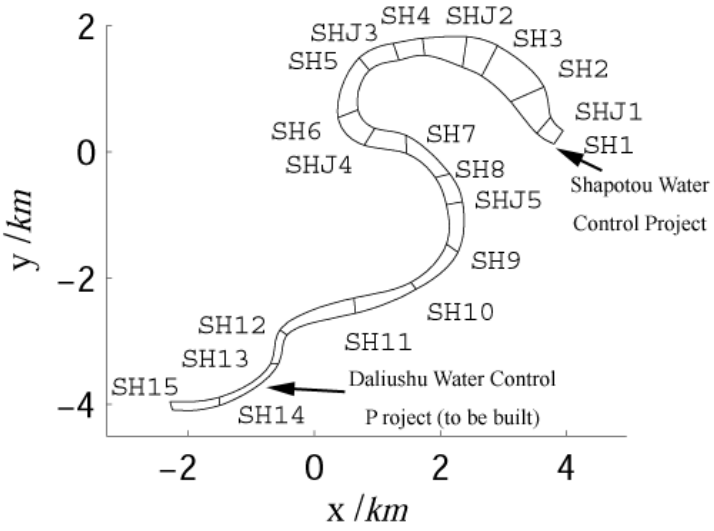

664

665 Figure 3 Plane view of Shapotou reservoir (The flow is in from SH15 and out from SH1, and the

666 direction of axis x is consistent with the east)

667

668

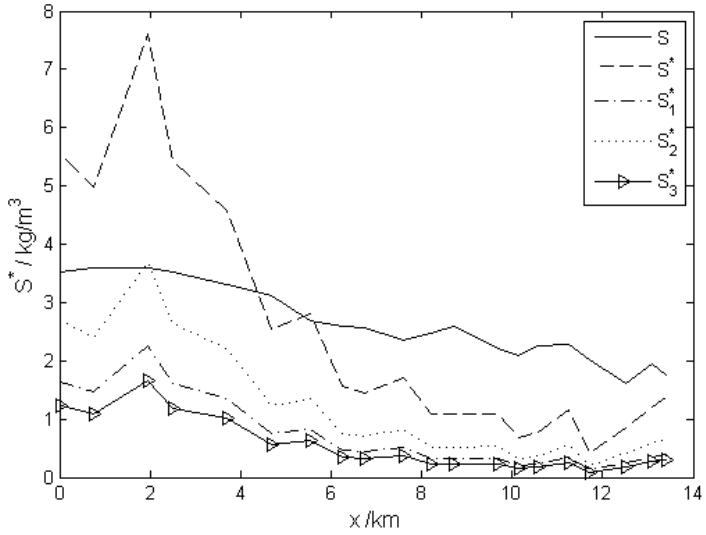

669

670 Figure 4 The distribution of total and group suspended sediment capacities(Case 2)

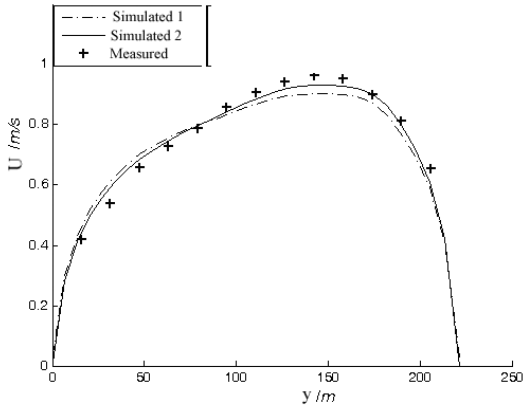

671

672 (1) SH7

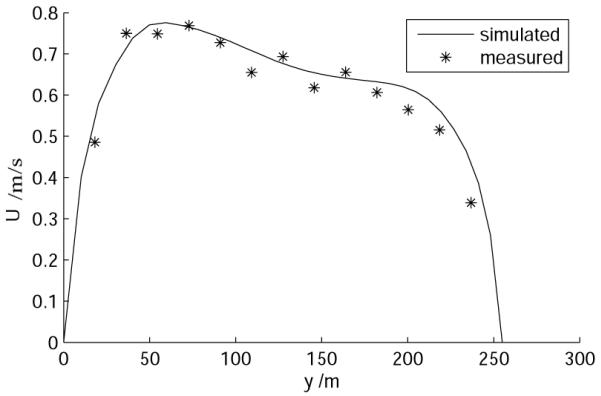

673

674 （2） SH5

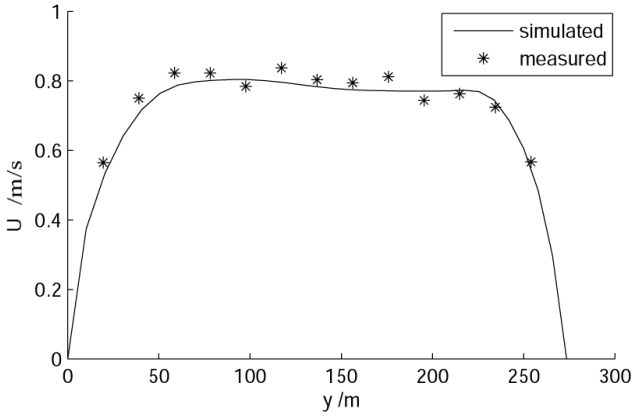

675

676 (3) SHJ2

677 Figure 5. Comparison of simulated and measured depth averaged velocities on three typical

678 cross-sections

679

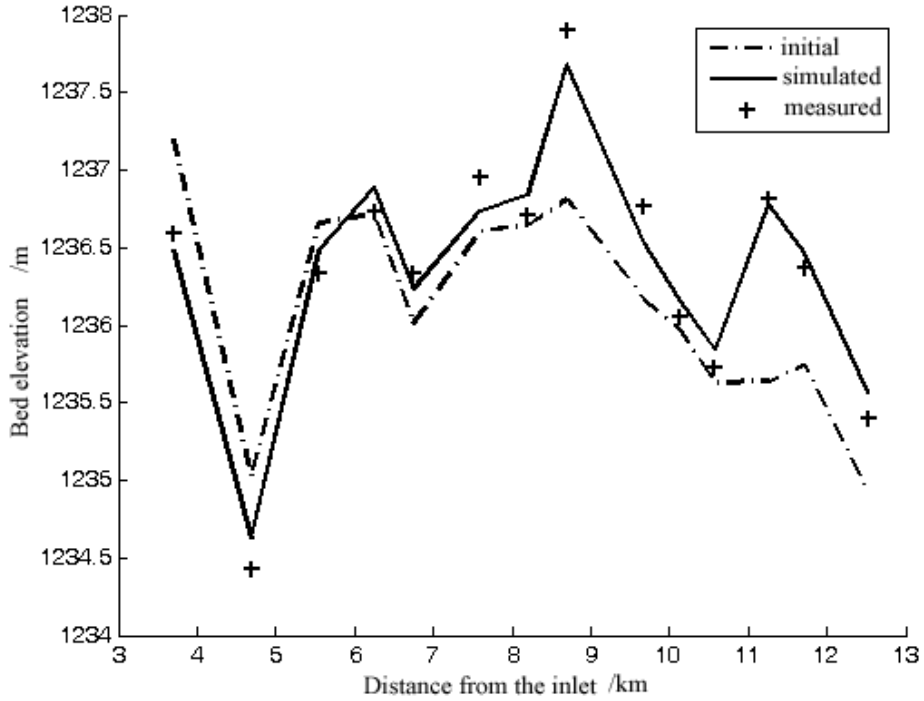

680

681 Figure 6 Comparison of simulated and measured bed elevation along the longitudinal direction

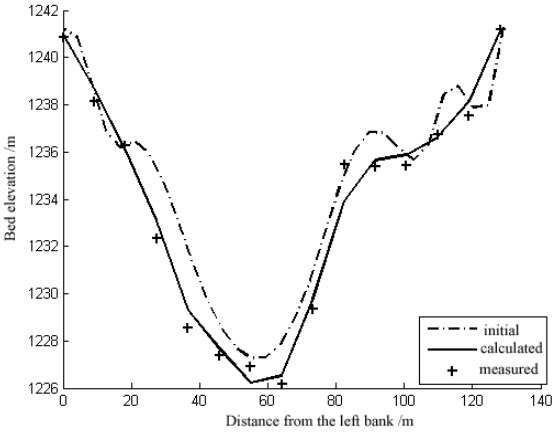

682

683 （1）SH10

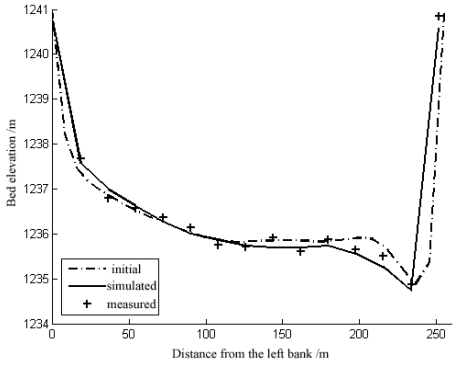

684

685 （2）SHJ5

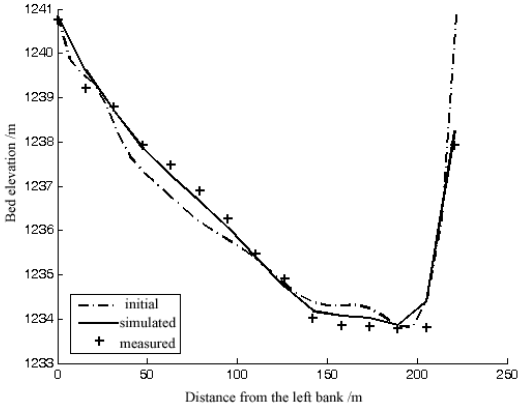

686

687 （3）SH7

688 Figure 7 Comparison of the measured and the simulated bed elevations on three typical cross

689 sections

690

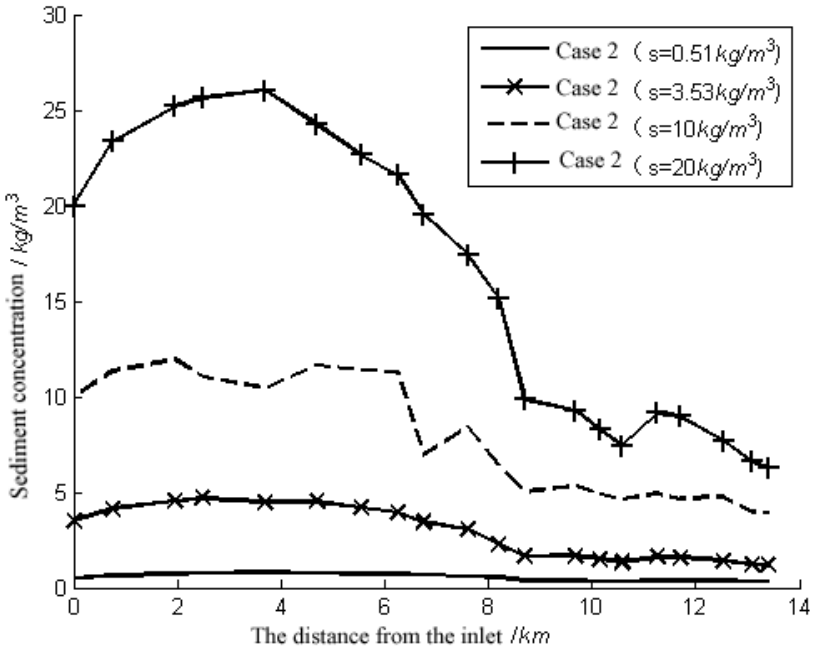

691

692 Figure 8 Distribution of suspended sediment concentration along the centerline of the studied

693 reach under the condition of Case 2

694

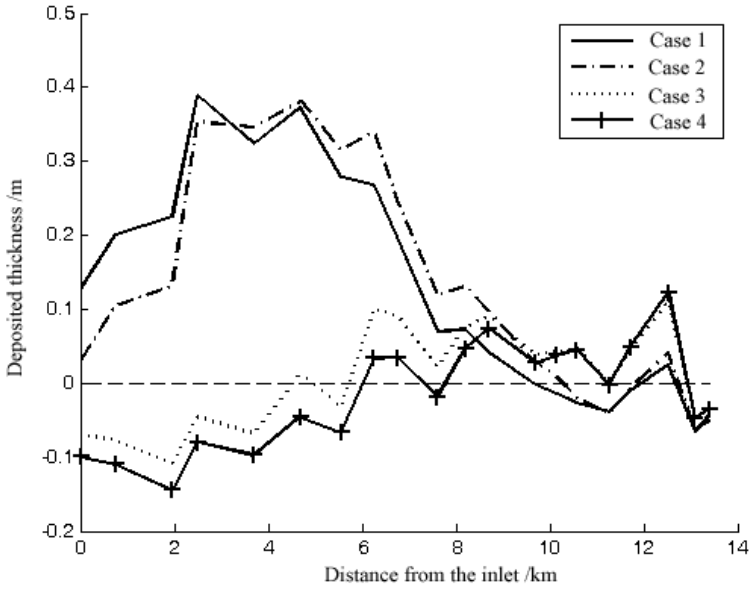

695

696 Figure 9 Comparison of the simulated bed deformations among the four cases with the same

697 sediment concentration（3.53kg/m^3）at the inlet

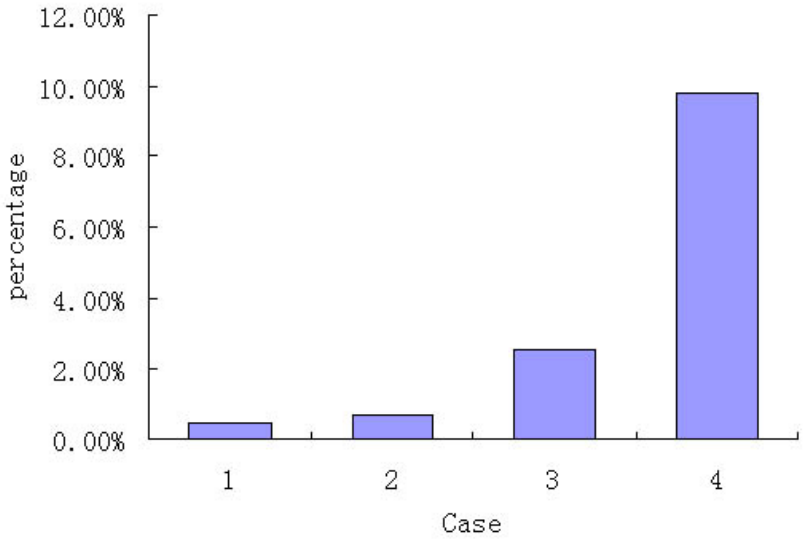

698

699 Figure 10 Percentage of bed deformation caused by bedload sediments in four cases

700

701

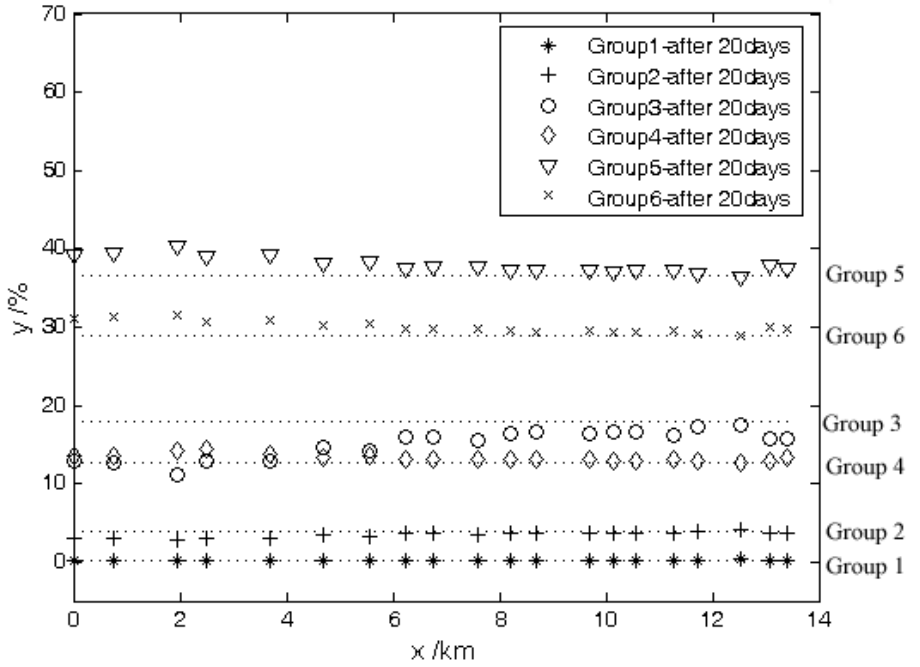

(a) S_{in}=0.51kg/m^3

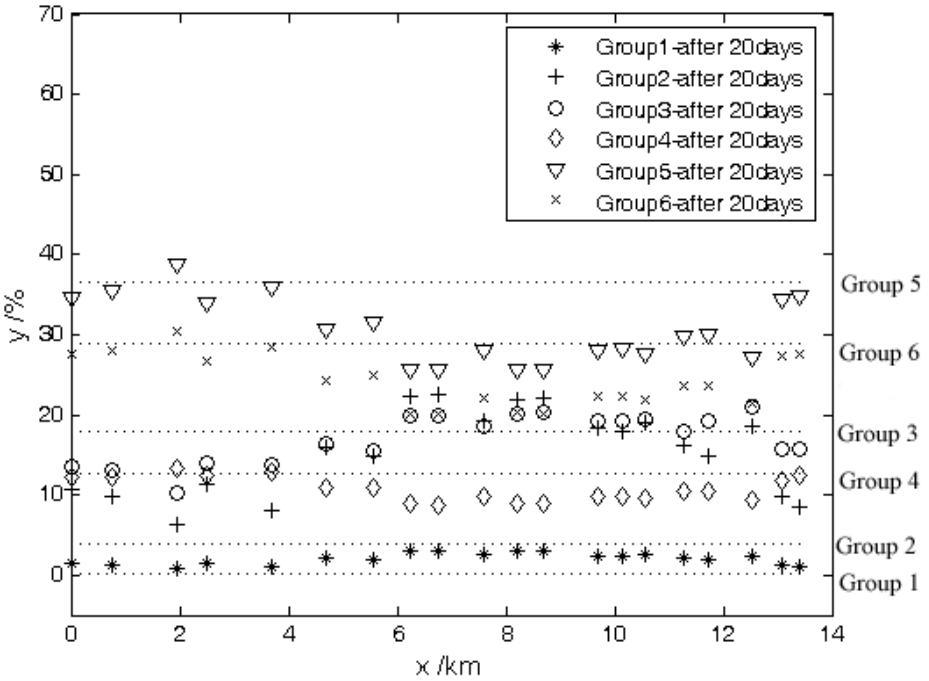

(b) S_{in}=10kg/m^3

Figure 11 The variation of effective bed material composition after 20 days